INTERNATIONAL JOURNAL FOR NUMERICAL METHODS IN ENGINEERING
Int. J. Numer. Meth. Engng 2012; **92**:79–98
Published online 6 June 2012 in Wiley Online Library (wileyonlinelibrary.com). DOI: 10.1002/nme.4330

A multiscale component mode synthesis approach for dynamic analysis of nanostructures

J. Lan and G. Li*,†

Department of Mechanical Engineering, Clemson University, Clemson, SC 29634-0921, USA

SUMMARY

A component mode synthesis-based multiscale approach is developed for dynamic analysis of nanostructures. The multiscale approach decomposes a nanostructure into atomistic and continuum regions and employs vibrational modes to connect the regions of different scales, enabling a reflectionless atomistic-to-continuum coupling. Dynamic response of the coupled atomistic and continuum regions is computed concurrently using a common time scale. Numerical results indicate that the multiscale approach has significant condensation and scaling advantages, and it is well suited for modeling and simulation of large and complex systems. Copyright © 2012 John Wiley & Sons, Ltd.

Received 13 July 2011; Accepted 7 March 2012

KEY WORDS: multiscale method; multiscale dynamics; component mode synthesis; lattice dynamics; atomistic-to-continuum coupling

1. INTRODUCTION

Over the past decade, multiscale methods have gained much interest because of the growing effort in capturing the physical phenomena occurring over a vast range of length scales. Comparing with pure atomistic approaches such as molecular dynamics and ab initio methods, multiscale methods are much more efficient, making them suitable to investigate large and complex systems. Since the early works by Kohlhoff and collaborators [1], many multiscale methods have been developed. Broadly defined, there are three multiscale modeling strategies: concurrent, top–down, and bottom–up approaches. Concurrent methods [2–8] typically decompose the physical domain into atomistic and continuum regions or layers. Atomistic and continuum calculations are performed simultaneously, and deformation-related information is exchanged between the atomistic and continuum regions/layers. Depending on the information exchange schemes, concurrent methods can be further categorized into domain bridging [2–4, 6], local enrichment [5], and multigrid [7, 8] methods. Top–down approaches, such as the quasicontinuum methods [9–12], the atomic-scale finite element method [13], and the heterogeneous multiscale method [14], solve the continuum equations by extracting constitutive laws from the underlying atomistic descriptions. In contrast, bottom–up methods such as the coarse-grained molecular dynamics [15, 16] coarse-grain the atoms of the system into macroatoms, and the fundamental equations defined on the atoms are coarse-grained into equivalent macroscale equations. Although these methods are successful in different aspects, many issues, such as artificial atom-continuum coupling effects, anharmonic effects, time scale mismatch, and so on, still remain to be addressed. Detailed discussions of various multiscale methods and existing issues can be found in several review articles [17–20].

*Correspondence to: G. Li, Department of Mechanical Engineering, Clemson University, Clemson, SC 29634-0921, USA.
†E-mail: gli@clemson.edu

In this paper, we introduce a multiscale component mode synthesis (CMS) approach for dynamic analysis of concurrent atomistic-continuum material systems. The CMS-based multiscale approach consists of a top–down component decomposition and a bottom–up CMS. At the component level, lattice dynamics is employed to compute the normal modes in the atomistic regions where 'nano effects' are significant. The normal modes are computed for the continuum regions by using continuum theories. A CMS technique is then employed to synthesize the normal modes of components to construct the global normal modes for the entire structure. At the global level, the constructed normal modes are used to generate a reduced-order system by using the mode superposition method to perform the dynamic analysis.

Different from other multiscale approaches, the CMS approach employs the vibrational modes to connect the atomistic and continuum regions. Through the mode synthesis procedure, the unimportant high-frequency waves are 'filtered out' instead of being reflected back. Thus, the artificial reflection of the high-frequency waves is completely eliminated. In addition, the combined global system has the same time scale in the continuum and atomistic regions. Relatively large time steps can be used in the dynamic analysis. Therefore, the time scale mismatch problem in conventional concurrent multiscale approaches is also eliminated. The CMS approach has significant condensation and scaling advantages, and it is well suited for modeling and simulation of large and complex systems. The method allows the individual substructures to be independently modeled, arbitrarily combined, and combined system response rapidly calculated to determine the global mechanical behavior. In addition, the substructuring and synthesis scheme is quite suitable for parallel computing. These advantageous numerical scaling properties enable the analysis of very large systems. Although in this work we use empirical potentials to model the interactions between the atoms and calculate the atomistic normal modes, more sophisticated atomistic models, such as ab initio models, can also be employed to calculate the atomic modes. For this reason, the proposed multiscale method is expandable in terms of adding atomistic physical models.

The rest of the paper is organized as follows. Section 2 presents the CMS-based multiscale method including a general description of the method, atomistic, and continuum dynamics theories and the CMS procedure to couple the atomistic and continuum models for the dynamic analysis. Section 3 shows multiscale dynamic analysis results for perfect and defective graphene structures subjected to external loadings. Conclusions are given in Section 4.

2. THEORY

2.1. General approach

Figure 1 illustrates the basic idea of the CMS-based multiscale analysis by using a simple example. Consider a nanostructure Ω that has some defects in the left part. As the mechanical effect of the defects can be significant because of the nanoscale size of the structure, the nanostructure is decomposed into an atomistic region, Ω^A, which contains the defects and a continuum region, Ω^C,

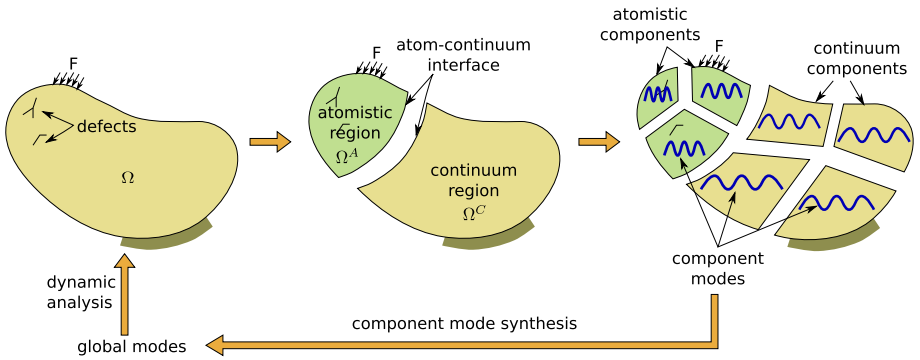

Figure 1. Schematic diagram of component mode synthesis-based multiscale dynamic analysis of a nanostructure.

DOI: 10.1002/nme

which is defect free. Atomistic models are employed for the atomistic region to describe the defects. In the continuum region where the material behavior is bulk-like, continuum theories are used to describe its mechanical response. Next, the atomistic and continuum regions are further decomposed into a set of atomistic and continuum components (or substructures) that are sufficiently small so that vibrational normal modes can be efficiently computed within each component.

In this work, once the component decomposition is completed, the normal modes of the atomistic components are computed by using the lattice dynamics theory. The normal modes of the continuum components are computed using linear elastodynamics theory and the spectral element method. The continuum and atomistic normal modes are then synthesized to form the global modes. The global normal modes are used in the standard mode superposition method to perform the dynamic analysis. Note that, only a few significant normal modes are retained in the CMS procedure and the rest are discarded, which ensures the efficiency of the top level mechanical analysis. In addition, although in this work we employ empirical potentials and lattice dynamics theory to compute the normal modes for the atomistic components, the multiscale CMS approach is a general technique in which more sophisticated atomistic models such as ab initio models [21] are equally applicable for describing the interaction of the atoms. Furthermore, in this work, the dynamic behavior of the nanostructures is modeled by a set of coupled linear equations of motion of the atoms and continuum elements. However, as there are many mode superposition techniques available for solving nonlinear dynamic problems [22, 23], it is expected that, by incorporating such techniques, the CMS-based multiscale approach may be extended for multiscale nonlinear dynamic analysis. We leave this topic to the future development of the CMS-based multiscale approach. In this paper, we focus on multiscale linear dynamic analysis of nanostructures.

2.2. Atomistic and continuum models

2.2.1. Lattice dynamics. In the theory of lattice dynamics [24], interatomic potentials are employed to describe the interactions between the atoms. Many interatomic potentials have been developed for different materials. For example, Lennard-Jones potential [25] and Morse potential [26] are among the two-body interatomic potentials. Popular many body potentials include Tersoff [27], Brenner [28], Stillinger-Weber [29] and many body Morse [30] potentials. In general, the total potential energy of a system of N atoms can be written as

$$U(\mathbf{x}) = \frac{1}{2}\sum_{\alpha\neq\beta} V_{\alpha\beta} \quad \alpha,\beta = 1,2,\ldots,N \tag{1}$$

where $\mathbf{x} = \{\mathbf{x}_1,\ldots,\mathbf{x}_N\}^T$ is the position vector of the N atoms, $V_{\alpha\beta}$ is the interatomic potential energy between the atoms α and β, and N is the number of atoms in the system. By using the harmonic approximation, the total potential energy of an N-atom system can be written in a quadratic form by neglecting the higher order (>2) terms in its Taylor's series expansion, that is,

$$U(\mathbf{x}) = U(\mathbf{X}) + \frac{1}{2}\sum_{\alpha,\beta=1}^{N}\sum_{i,j=1}^{3}\left.\frac{\partial^2 U(\mathbf{x})}{\partial \mathbf{u}_{\alpha i}\partial \mathbf{u}_{\beta j}}\right|_{\mathbf{x}_1,\ldots,\mathbf{x}_N=\mathbf{X}_1,\ldots,\mathbf{X}_N} \mathbf{u}_{\alpha i}\mathbf{u}_{\beta j} \quad i,j=1,2,3 \tag{2}$$

where $\mathbf{X} = \{\mathbf{X}_1,\ldots,\mathbf{X}_N\}^T$ is the initial equilibrium position vector of the atoms, $\mathbf{u}_{\alpha i}$ and $\mathbf{u}_{\beta j}$ are the i-th and j-th components of the displacement of the atoms α and β, respectively. Equation (2) can be rewritten in a matrix form as

$$U(\mathbf{x}) = U(\mathbf{X}) + \frac{1}{2}\mathbf{u}^T\mathbf{K}\mathbf{u} \tag{3}$$

where $\mathbf{u} = \{\mathbf{u}_1,\ldots,\mathbf{u}_N\}^T$ and $\mathbf{K}$ is the $3N\times 3N$ force constant matrix given by

$$\mathbf{K}_{3\alpha+i-3,3\beta+j-3} = \left.\frac{\partial^2 U(\mathbf{X}+\mathbf{u})}{\partial \mathbf{u}_{\alpha i}\partial \mathbf{u}_{\beta j}}\right|_{\mathbf{u}=\mathbf{0}} \quad \alpha,\beta = 1,\ldots,N, \quad i,j=1,2,3. \tag{4}$$

DOI: 10.1002/nme

The equation of motion of the atoms is obtained as

$$\mathbf{M}\ddot{\mathbf{u}} + \mathbf{K}\mathbf{u} = \mathbf{F}_{\text{ext}} \tag{5}$$

where $\mathbf{M}$ is the $3N \times 3N$ diagonal mass matrix, $\ddot{\mathbf{u}}$ is the acceleration vector of the atoms, and $\mathbf{F}_{\text{ext}}$ is the external force vector. For free vibrations, by taking the harmonic time dependence for all the atoms, the equation of motion can be written as [24]

$$\left(\mathbf{K} - \omega^2\mathbf{M}\right)\mathbf{d} = 0 \tag{6}$$

where the eigenvalues, ω, and eigenvectors, $\mathbf{d}$, of the generalized eigenvalue problem are the phonon frequencies and normal modes of the system, respectively. Note that the equation of motion given in Equation (5) does not include thermal fluctuation of the atoms. To account for the temperature effect, one can employ the Langevin equation of motion in which a dissipative friction force and a random force due to thermal fluctuation are added to Equation (5) [31, 32]. For a system with a large number of atoms, direct time integration of Equation (5) becomes very expensive. However, because the direct approach provides the all-atom solution of the nanostructures, in this paper, the solution from the direct approach is used as the reference for comparison with the results from the CMS-based multiscale approach.

2.2.2. Linear continuum elastodynamics. In the theory of linear continuum elastodynamics, the overall potential energy of the structure is expressed as an integral of a strain energy density function W over the continuum volume Ω^c of the body,

$$U = \int_{\Omega^C} W(\mathbf{x})\mathrm{d}\Omega. \tag{7}$$

The strain energy density is given by

$$W(\mathbf{x}) = \frac{1}{2}\boldsymbol{\sigma}(\mathbf{x})^T\boldsymbol{\epsilon}(\mathbf{x}) = \frac{1}{2}\boldsymbol{\epsilon}(\mathbf{x})^T\mathbf{C}\boldsymbol{\epsilon}(\mathbf{x}) \tag{8}$$

where $\boldsymbol{\sigma}$ is the stress vector corresponding to the strain vector $\boldsymbol{\epsilon}$ for a linear homogeneous isotropic elastic solid and $\mathbf{C}$ is the material tensor containing the elastic constants. From the first law of thermal dynamics, the mechanical energy equation can be written as

$$\frac{D}{Dt}(K + U) = P_{\text{ext}} \tag{9}$$

where K is the kinetic energy and P_{ext} is the external mechanical power. K and P_{ext} are defined as

$$K = \int_{\Omega^C} \frac{1}{2}\rho\mathbf{v}^T\mathbf{v}\mathrm{d}\Omega \tag{10}$$

$$P_{\text{ext}} = \int_{\partial\Omega^C} \mathbf{v}^T\mathbf{t}\mathrm{d}S + \int_{\Omega^C} \mathbf{v}^T\mathbf{b}\mathrm{d}\Omega \tag{11}$$

where ρ is the mass density of the material, $\mathbf{v}$ is the velocity, $\mathbf{t}$ is the surface traction, and $\mathbf{b}$ is the body force density. By substituting Equations (7), (10), and (11) into Equation (9), we obtain the continuum equation of motion as

$$\int_{\Omega^C} \rho\mathbf{v}^T\dot{\mathbf{v}}\mathrm{d}\Omega + \int_{\Omega^C} \boldsymbol{\epsilon}\mathbf{C}\dot{\boldsymbol{\epsilon}}\mathrm{d}\Omega = \int_{\partial\Omega^C} \mathbf{v}^T\mathbf{t}\mathrm{d}S + \int_{\Omega^C} \mathbf{v}^T\mathbf{b}\mathrm{d}\Omega \tag{12}$$

Equation (12) can be solved using numerical methods such as the finite element and spectral element methods. In these methods, the field variables such as the position $\mathbf{x}$, displacement $\mathbf{u}$, velocity $\mathbf{v}$, and acceleration $\mathbf{a}$ within each element can be interpolated from the nodal values $(\mathbf{x}_i, \mathbf{u}_i, \mathbf{v}_i, \mathbf{a}_i)$, $i = 1, 2, \ldots, n$, through a set of shape functions $S_i(\mathbf{x})$, $i = 1, 2, \ldots, n$, as

$$\mathbf{x} = \sum_{i=1}^{n} S_i(\mathbf{x})\mathbf{x}_i, \quad \mathbf{u} = \sum_{i=1}^{n} S_i(\mathbf{x})\mathbf{u}_i, \quad \mathbf{v} = \sum_{i=1}^{n} S_i(\mathbf{x})\mathbf{v}_i, \quad \mathbf{a} = \sum_{i=1}^{n} S_i(\mathbf{x})\mathbf{a}_i \tag{13}$$

DOI: 10.1002/nme

where n is the number of nodes in an element and i denotes the i-th node. For clarity of notation, in this paper, we use the same set of symbols to denote the mechanical quantities such as position $\mathbf{x}$ and displacement $\mathbf{u}$ for both atoms and nodes when the meaning of the notations can be clearly determined from the context. Substituting Equation (13) into (12) and carrying out numerical integration, one obtains

$$\mathbf{v}^T(\mathbf{Ma} + \mathbf{Ku}) = \mathbf{v}^T\mathbf{F}_{\text{ext}} \tag{14}$$

where $\mathbf{M}$ is the mass matrix, $\mathbf{K}$ is the stiffness matrix, and $\mathbf{F}_{\text{ext}}$ is the external force vector. For a nontrivial nodal velocity $\mathbf{v}$ in Equation (14), the equation of motion implies

$$\mathbf{M\ddot{u}} + \mathbf{Ku} = \mathbf{F}_{\text{ext}} \tag{15}$$

where $\mathbf{u}$ is the global nodal displacement vector and $\ddot{\mathbf{u}} = \mathbf{a}$. For free vibrations, by taking the harmonic time dependence for the nodal displacements, the equation of motion can be written as

$$\left(\mathbf{K} - \omega^2\mathbf{M}\right)\mathbf{d} = \mathbf{0} \tag{16}$$

where ω is the natural frequency and $\mathbf{d}$ is the normal mode of the system. Because in the CMS-based multiscale approach, Equation (16) needs to be solved for each component to obtain the component normal modes; the spectral element method [33] is advantageous because of the fact that the mass matrix produced by spectral element is inherently diagonal. In addition, as a high-order domain decomposition method that combines the competitive advantages of low-order finite element and high-order spectral methods [33, 34], the spectral element method not only has highly flexible domain decomposition capability but also has exponential convergence characteristics and built-in p-refinement capability [35, 36]. Therefore, we employ the spectral element method for solving the continuum equations.

In the spectral element method, each element is further discretized by a set of Gauss-Lobatto-Legendre (GLL) collocation points. In two dimensions, a square master element is typically discretized into $P \times Q$ GLL collocation points in the x-direction and y-direction. The two-dimensional shape functions $S_i(x, y)$, $i = 1, 2, \ldots, n$, $n = P \times Q$, for the master element are the tensor product of one-dimensional Lagrange interpolants $l_m^P(x)$ and $l_m^Q(y)$ defined on these GLL collocation points. The Lagrange interpolants $l_m^P(x)$ and $l_m^Q(y)$ are given, respectively, by

$$l_m^P(x) = \frac{-\left(1-x^2\right)L'_P(x)}{P(P+1)L_P(x_m)(x-x_m)}, \quad m = 1, 2, \ldots, P \tag{17}$$

$$l_m^Q(y) = \frac{-\left(1-y^2\right)L'_Q(y)}{Q(Q+1)L_Q(y_m)(y-y_m)}, \quad m = 1, 2, \ldots, Q \tag{18}$$

where L_P and L'_P are the P-th order Legendre polynomial and its derivative, respectively. Standard isoparametric mapping can be used for general quadrilateral elements. Three-dimensional spectral shape functions can be constructed similarly.

2.3. Multiscale component mode synthesis approach

Since the CMS method was first introduced by Hurty in 1965 [37], it has been frequently used to analyze large structures such as vehicles and space shuttles and has also been the subject of research in different areas (see e.g. [38–40] and references therein). The most appreciated advantage of CMS approach is that it can represent the many degrees of freedom of a component by a much smaller number of component modes. In this work, the CMS method is extended to connect the atomistic and continuum regions through the normal modes. In the following, we present the details of the CMS-based multiscale approach by using an example shown in Figure 2.

Consider a multiscale model of a graphene sheet as shown in Figure 2. In the left region are the carbon atoms connected by the bonds. The right region of the graphene is modeled as a continuum medium that is represented by a set of spectral elements. In the CMS approach, the global model in Figure 2 is first decomposed into a set of components. By using A and C to denote the atomistic

DOI: 10.1002/nme

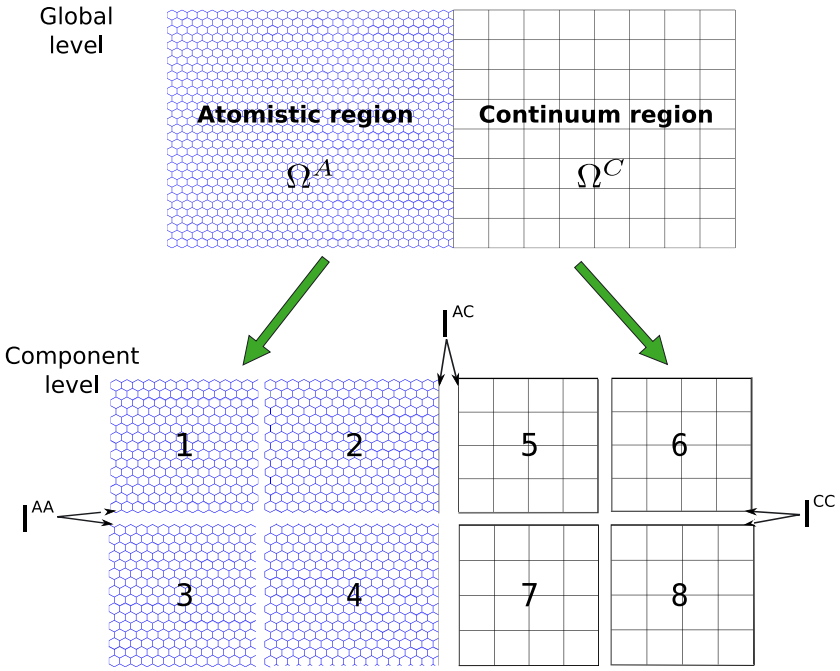

Figure 2. Component decomposition of a graphene.

and continuum components, respectively, I^{AA}, I^{CC}, and I^{AC} are referred to as the atom–atom, continuum–continuum, and atom–continuum component interfaces, respectively. Then, the general eigenvalue problems given in Equations (6) and (16) become

$$\left(\mathbf{K}^{t,j} - \lambda^{t,j}\mathbf{M}^{t,j}\right)\mathbf{d}^{t,j} = 0, \quad j = 1, 2, \ldots, m^t, \quad t = A \text{ or } C \tag{19}$$

where t denotes the type of the component (A, atomistic; C, continuum), j denotes the j-th component, m^t is the total number of the components of type t, λ denotes the eigenvalue of the system that is the square of the frequency ω, and $\mathbf{d}$ denotes the normal mode of the system. Following Craig–Bampton's decomposition [41], the DOFs of a component are partitioned into two parts that are referred to as the attachment part and omitted part. The attachment DOFs represent the DOFs of the atoms or nodes on interface edges that are shared by neighbor components, whereas the rest of the DOFs of a component are referred to as the omitted DOFs. The attachment and omitted parts of the DOFs are denoted by subscripts a and o, respectively. With respect to the attachment and omitted DOFs, Equation (19) can be partitioned as

$$\left(\begin{bmatrix} \mathbf{K}_{oo}^{t,j} & \mathbf{K}_{oa}^{t,j} \\ \mathbf{K}_{ao}^{t,j} & \mathbf{K}_{aa}^{t,j} \end{bmatrix} - \lambda^{t,j}\begin{bmatrix} \mathbf{M}_{oo}^{t,j} & \mathbf{M}_{oa}^{t,j} \\ \mathbf{M}_{ao}^{t,j} & \mathbf{M}_{aa}^{t,j} \end{bmatrix}\right)\begin{Bmatrix} \mathbf{d}_o^{t,j} \\ \mathbf{d}_a^{t,j} \end{Bmatrix} = \begin{Bmatrix} \mathbf{0} \\ \mathbf{0} \end{Bmatrix} \tag{20}$$

The interior component modes of a component can be obtained by fixing all the attachment DOFs, that is, $\mathbf{d}_a^{t,j} = 0$, and solving an eigenvalue problem of the form

$$\left(\mathbf{K}_{oo}^{t,j} - \lambda^{t,j}\mathbf{M}_{oo}^{t,j}\right)\mathbf{d}_o^{t,j} = \mathbf{0} \tag{21}$$

The eigenpairs $\left(\lambda^{t,j}, \mathbf{d}_o^{t,j}\right)$ can thus be computed from Equation (21). Note that when a component edge is also a part of the global boundary where a Dirichlet boundary condition is applied, the boundary condition should be applied when solving Equation (21). In the CMS approach, only a small set of $\mathbf{d}_o^{t,j}$ corresponding to the lower frequencies is retained and assembled column-wisely into the interior modal matrix $\mathbf{D}_o^{t,j}$, that is,

$$\mathbf{D}_o^{t,j} = \left[\mathbf{d}_{o1}^{t,j} \;\; \mathbf{d}_{o2}^{t,j} \;\; \ldots \;\; \mathbf{d}_{ok}^{t,j}\right] \tag{22}$$

DOI: 10.1002/nme

The number of modes retained, k, is typically less than the DOFs of the component because within each component, the higher order component modes do not contribute much to the global mechanical behavior of the structure. Next, a set of constraint modes of the components is obtained by a static analysis using the stiffness matrix of the component with attachment DOFs included. The purpose of the static constraint modes lies in two folds: first, the constraint modes serve as a part of the Ritz basis vectors for the approximation of the component displacement, and second, they are the modes connecting the neighboring components. There are several approaches in the CMS literature for obtaining the constraint modes [41–43]. In this work, we adopt the unit displacement approach [41]. It is shown in Section 3 that this approach is sufficient to yield satisfactory results. Applying a unit displacement on the attachment DOFs, the equations of motion of the atomistic and continuum components, Equations (5) and (15), can be rewritten in a static analysis as the following equation of equilibrium:

$$\begin{bmatrix} \mathbf{K}_{oo}^{t,j} & \mathbf{K}_{oa}^{t,j} \\ \mathbf{K}_{ao}^{t,j} & \mathbf{K}_{aa}^{t,j} \end{bmatrix} \begin{bmatrix} \boldsymbol{\Psi}_o^{t,j} \\ \mathbf{I}_a \end{bmatrix} = \begin{bmatrix} \mathbf{0} \\ \mathbf{R}_a^{t,j} \end{bmatrix}, \tag{23}$$

where each column of the identity matrix $\mathbf{I}_a$ is used to enforce a unit displacement on one attachment (or interface) atom or node with the other attachment atoms or nodes fixed. $\mathbf{R}_a$ is the resultant vector of reaction at the attachment atoms or nodes. $\boldsymbol{\Psi}_o$ is the displacement of the omitted atoms or nodes because of the applied unit displacement on the attachment atoms or nodes. $\boldsymbol{\Psi}_o$ can be obtained from Equation (23) explicitly as

$$\boldsymbol{\Psi}_o^{t,j} = -\left(\mathbf{K}_{oo}^{t,j}\right)^{-1} \mathbf{K}_{oa}^{t,j} \ . \tag{24}$$

After $\boldsymbol{\Psi}_o^{t,j}$ is obtained, it can be used along with the modal matrix obtained in Equation (22) to form a Ritz basis set. The normal modes in Equation (19) can be represented as a linear combination of the Ritz basis vectors, that is,

$$\mathbf{d}^{t,j} = \begin{bmatrix} \mathbf{D}_o^{t,j} & \boldsymbol{\Psi}_o^{t,j} \\ \mathbf{0} & \mathbf{I}_a \end{bmatrix} \begin{Bmatrix} \mathbf{a}^{t,j} \\ \mathbf{d}_a^{t,j} \end{Bmatrix} = \mathbf{T}^{t,j} \mathbf{z}^{t,j} \tag{25}$$

where $\mathbf{T}^{t,j}$ is the transformation matrix of component j of type t. The columns in the transformation matrix are the Ritz basis vectors. The columns corresponding to $\mathbf{D}_o^{t,j}$ and $\boldsymbol{\Psi}_o^{t,j}$ are the interior and constraint component modes, respectively. The transformation matrix is rectangular with the number of columns (i.e., number of retained Ritz basis vectors) less than the DOFs of the component. This model order reduction technique of CMS eliminates the high-order modes of the components, especially those in the atomistic components, and largely reduces the DOFs of the system.

A major difficulty arises in the coupling of the atomistic and continuum components. As shown in Figure 2, there are three types of interfaces in the domain: I^{AA}, I^{CC}, and I^{AC}. If a component only contains interfaces of type I^{AA} or I^{CC}, it is compatible with its neighbor components. The components 1, 3, 6, and 8 in Figure 2 are such components. These components share the same set of atoms or nodes with their neighbor components. For such components, $\boldsymbol{\Psi}_o^{t,j}$ is directly computed by using Equations (23) and (24). Nevertheless, for components that have an interface edge of I^{AC} type, such as components 2, 4, 5, and 7 in Figure 2, the attachment DOFs of the atomistic component and its neighbor continuum component(s) are typically not conforming on I^{AC} because of the different length scales of atomic lattice and continuum elements. Although it is possible to mesh the continuum part such that the continuum nodes are coincident with the atoms, the continuum meshing process can be rather complicated to scale down the nodal spacing to atomic bond length at the atom–continuum interfaces. A large number of elements may be required in some cases, which impairs the scaling advantage of the multiscale coupling. Furthermore, it can be a severe obstacle in three dimensions [44]. For these reasons, in our approach, nonconforming atom–continuum interfaces are allowed, and the continuum regions of the nanostructure can be meshed freely. For nonconforming atom–continuum interfaces, numerical treatment is needed for the displacement

DOI: 10.1002/nme

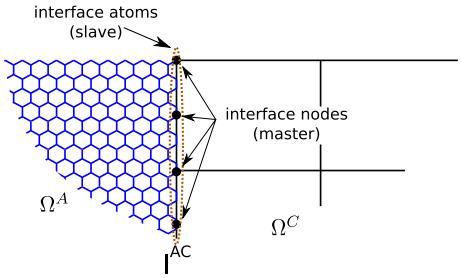

Figure 3. Atom–continuum coupling model.

transition between the atoms and continuum nodes on or near the interface, which leads to a modified version of Equations (23) and (24) for the calculation of $\mathbf{\Psi}_o^{t,j}$. Several displacement transition schemes have been proposed in the literature [20, 45]. Here, we use a pointwise master-slave coupling method (also known as the constrained approximation) [46, 47] to couple the displacement between the atomistic and the continuum components. As shown in Figure 3, the atoms on the I^{AC} interface are treated as slaves, and the nodes are regarded as masters. The displacement of the atoms on the interface is interpolated by

$$\mathbf{u}_j^A = \sum_{i=1}^{n} S_i\left(\mathbf{x}_j^A\right)\mathbf{u}_i^C, \quad i = 1, 2, .., n \tag{26}$$

where $\mathbf{u}_j^A$ is the displacement of atom j on the interface, $S_i\left(\mathbf{x}_j^A\right)$, $i = 1, 2, .., n$, are the shape functions of the spectral element evaluated at the position of atom j (i.e., $\mathbf{x}_j^A$), $\mathbf{u}_i^C$ is the displacement of node i in the element, and n is the number of nodes in the spectral element.

Using this master-slave coupling method, the displacement of the atoms on the interface is represented by that of the spectral nodes. For the continuum components 5 and 7 in Figure 2, as their attachment DOFs on the interface I^{AC}, $\mathbf{d}_a^{C,j}(AC)$, are master DOFs, the constraint modes are still computed by using Equations (23) and (24). For the atomistic components 2 and 4 shown in Figure 2, the attachment DOFs are partitioned into atom–atom attachment DOFs, $\mathbf{d}_a^{A,j}(AA)$, and atom–continuum attachment DOFs, $\mathbf{d}_a^{A,j}(AC)$. Then, the slave atom–continuum attachment DOFs, $\mathbf{d}_a^{A,j}(AC)$, on the interface I^{AC} are interpolated by $\mathbf{d}_a^{C,j}(AC)$ as shown in Equation (26). The component mode

$$\mathbf{d}^{A,j} = \begin{Bmatrix} \mathbf{d}_o^{A,j} \\ \mathbf{d}_a^{A,j} \end{Bmatrix} = \begin{Bmatrix} \mathbf{d}_o^{A,j} \\ \mathbf{d}_a^{A,j}(AA) \\ \mathbf{d}_a^{A,j}(AC) \end{Bmatrix} = \begin{bmatrix} \mathbf{I} & & \\ & \mathbf{I} & \\ & & \mathbf{S} \end{bmatrix} \begin{Bmatrix} \mathbf{d}_i^{A,j} \\ \mathbf{d}_a^{A,j}(AA) \\ \mathbf{d}_a^{C,j}(AC) \end{Bmatrix} \tag{27}$$

where $\mathbf{I}$ is the identity matrix and $\mathbf{S}$ is the shape function matrix of the neighbor spectral elements evaluated at the atoms on the interface I^{AC}. By using Equation (27), the slave atomistic attachment DOFs, $\mathbf{d}_a^{A,j}(AC)$, on I^{AC} are condensed out and replaced by the master continuum attachment DOFs, $\mathbf{d}_a^{C,j}(AC)$. Through this procedure, as will be shown later in this section, component matrices of the atomistic and continuum components can be assembled together through the shared attachment DOFs, $\mathbf{d}_a^{C,j}(AC)$. Denoting

$$\bar{\mathbf{S}} = \begin{bmatrix} \mathbf{I} & & \\ & \mathbf{I} & \\ & & \mathbf{S} \end{bmatrix}, \tag{28}$$

and substituting Equation (27) into Equation (19), Equation (19) can be rewritten as

$$\left(\bar{\mathbf{S}}^T\mathbf{K}^{A,j}\bar{\mathbf{S}} - \lambda^{A,j}\bar{\mathbf{S}}^T\mathbf{M}^{A,j}\bar{\mathbf{S}}\right)\bar{\mathbf{d}}^{A,j} = \mathbf{0}. \tag{29}$$

In short form,

$$\left(\bar{\mathbf{K}}^{A,j} - \lambda^{A,j}\bar{\mathbf{M}}^{A,j}\right)\bar{\mathbf{d}}^{A,j} = \mathbf{0} \tag{30}$$

DOI: 10.1002/nme

where $\bar{\mathbf{K}}^{A,j} = \bar{\mathbf{S}}^T \mathbf{K}^{A,j} \bar{\mathbf{S}}$ and $\bar{\mathbf{M}}^{A,j} = \bar{\mathbf{S}}^T \mathbf{M}^{A,j} \bar{\mathbf{S}}$ are the new stiffness matrix and mass matrix. Once again, by partitioning the matrices according to the omitted and new attachment DOFs, one obtains a modified version of Equation (23) as

$$\begin{bmatrix} \bar{\mathbf{K}}_{oo}^{A,j} & \bar{\mathbf{K}}_{oa}^{A,j} \\ \bar{\mathbf{K}}_{ao}^{A,j} & \bar{\mathbf{K}}_{aa}^{A,j} \end{bmatrix} \begin{bmatrix} \boldsymbol{\Psi}_o^{A,j} \\ \mathbf{I}_a \end{bmatrix} = \begin{bmatrix} \mathbf{0} \\ \mathbf{R}_a^{A,j} \end{bmatrix}. \tag{31}$$

Then, $\boldsymbol{\Psi}_o^{A,j}$ can be obtained as

$$\boldsymbol{\Psi}_o^{A,j} = -\left(\bar{\mathbf{K}}_{oo}^{A,j}\right)^{-1} \bar{\mathbf{K}}_{oa}^{A,j}. \tag{32}$$

Because the displacement interpolation is carried out on the interface, it can be shown that $\mathbf{K}_{oo}^{A,j}$ remains the same after the interpolation, that is, $\bar{\mathbf{K}}_{oo}^{A,j} = \mathbf{K}_{oo}^{A,j}$. Therefore, Equation (21) remains the same for all the components. In summary, for atomistic components containing an interface of type I^{AC}, the interior component modes, $\begin{Bmatrix} \mathbf{D}_o^{A,j} \\ \mathbf{0} \end{Bmatrix}$, are computed by Equations (21) and (22), and the constraint modes, $\begin{Bmatrix} \boldsymbol{\Psi}_o^{A,j} \\ \mathbf{I}_a \end{Bmatrix}$, are computed by Equation (32). For all the other components, the interior component modes are computed by Equations (21) and (22), and the constraint modes are computed by Equation (24).

Once the component modes are computed and the transformation matrix $\mathbf{T}$ shown in Equation (25) is obtained, the component equations of motion, Equations (5) and (15), can be reduced to

$$\mathbf{M}_r^{t,j} \ddot{\mathbf{q}}^{t,j} + \mathbf{K}_r^{t,j} \mathbf{q}^{t,j} = \mathbf{R}_r^{t,j} \tag{33}$$

where $\mathbf{K}_r^{t,j} = \mathbf{T}^{t,j\,T} \mathbf{K}^{t,j} \mathbf{T}^{t,j}$, $\mathbf{M}_r^{t,j} = \mathbf{T}^{t,j\,T} \mathbf{M}^{t,j} \mathbf{T}^{t,j}$, and $\mathbf{R}_r^{t,j} = \mathbf{T}^{t,j\,T} \mathbf{R}^{t,j}$ are the reduced component stiffness, mass matrices, and the force vector, respectively. Following the standard finite element assembly procedure, one can assemble the reduced component equations of motion into a system where the reduced global stiffness matrix $\mathbf{K}_r$, mass matrix $\mathbf{M}_r$, and force vector $\mathbf{R}_r$ can be obtained as

$$\mathbf{M}_r = \bigcup_{t,j} \mathbf{M}_r^{t,j}, \quad \mathbf{K}_r = \bigcup_{t,j} \mathbf{K}_r^{t,j}, \quad \mathbf{R}_r = \bigcup_{t,j} \mathbf{R}_r^{t,j}. \tag{34}$$

The reduced global equation of motion can be written as

$$\mathbf{M}_r \ddot{\mathbf{q}} + \mathbf{K}_r \mathbf{q} = \mathbf{R}_r. \tag{35}$$

Although Equation (35) can be solved by using various time integration schemes (e.g., the Newmark Scheme), the mode superposition method can be employed to further reduce the complexity and computational cost of the dynamic analysis. By solving the free vibration problem corresponding to Equation (35),

$$\mathbf{K}_r \mathbf{b} = \lambda \mathbf{M}_r \mathbf{b}, \tag{36}$$

the global generalized coordinate vector $\mathbf{q}$ can be closely approximated by the first a few normal modes as

$$\mathbf{q} = \sum_{n=1}^{p} \mathbf{b}_n s_n = \mathbf{B}\mathbf{s}, \tag{37}$$

where p is the number of selected global normal modes, $\mathbf{B}$ is the transformation matrix whose columns are the chosen normal modes $\mathbf{b}_n$, and $\mathbf{s}$ is the vector of the new generalized coordinates. Substituting Equation (37) into Equation (35) and premultiplying $\mathbf{B}^T$ to both sides, the final decoupled equation of motion can be obtained as

$$\ddot{\mathbf{s}} + \lambda \mathbf{s} = \mathbf{B}^T \mathbf{R}_r. \tag{38}$$

DOI: 10.1002/nme

Equation (38) can be solved very efficiently because the dimension of the system is small. Once **s** is computed from Equation (38), the global displacement vector including both atomic and nodal displacements can be obtained using the transformation matrices, that is,

$$\mathbf{u} = \mathbf{TBs}. \tag{39}$$

3. RESULTS AND DISCUSSION

To investigate the performance of the CMS-based multiscale approach for dynamic analysis of nanostructures, we investigate the dynamic behavior of perfect and defective graphene structures subjected external forces. We first consider a perfect graphene with a length of 27.085 nm and a width of 6.533 nm. As shown in Figure 4, the left edge of the graphene is fixed, and two types of forces are applied on the right edge: a uniform horizontal loading (stretching case) and a uniform vertical loading (bending case). In the stretching case, the distributed force acting on the right edge of the graphene is 2449.1 pN/nm, and in the bending case, the distributed force along the right edge is 244.9 pN/nm. There are a total of 7232 atoms in the graphene.

In this work, the interaction between the carbon atoms in the graphene structure is modeled by a multibody modified Morse potential [30], that is,

$$V_{\alpha\beta} = V_{\alpha\beta}^{\text{stretch}} + V_{\alpha\beta}^{\text{angle}} \tag{40}$$

$$V_{\alpha\beta}^{\text{stretch}} = D_e \left\{ \left[1 - e^{-\eta[r_{\alpha\beta} - r_0]} \right]^2 - 1 \right\} \tag{41}$$

$$V_{\alpha\beta}^{\text{angle}} = \sum_{\gamma \neq \alpha,\beta} \frac{1}{2} k_\theta \left(\theta_{\alpha\beta\gamma} - \theta_0 \right)^2 \left[1 + k_{\text{sextic}} \left(\theta_{\alpha\beta\gamma} - \theta_0 \right)^4 \right], \tag{42}$$

where $V_{\alpha\beta}^{\text{stretch}}$ is the bond stretch energy between atoms α and β, $V_{\alpha\beta}^{\text{angle}}$ is the energy due to bond angle change between the bond $\alpha - \beta$ and its adjacent bonds, $r_{\alpha\beta}$ is the length of the bond $\alpha\beta$, $\theta_{\alpha\beta\gamma}$ is the angle between bonds $\alpha\beta$ and $\alpha\gamma$, and r_0 and θ_0 are the undeformed bond length and angle, respectively. The parameters for graphene are given by [30]:

$$r_0 = 1.39 \times 10^{-10} \text{ m}, \quad D_e = 6.03105 \times 10^{-19} \text{ N} \cdot \text{m}, \quad \eta = 2.625 \times 10^{10} \text{ m}^{-1}$$

$$\theta_0 = 2.094 \text{ rad}, \quad k_\theta = 0.9 \times 10^{-18} \text{ N} \cdot \text{m/rad}^2, \quad k_{\text{sextic}} = 0.754 \text{ rad}^{-4}$$

The multiscale model of the graphene is shown in Figure 5 in which the right part of the structure is modeled as a continuum region. The sizes of the atomistic and continuum regions are 6.862 nm ×6.533 nm and 20.224 nm ×6.533 nm, respectively. The Young's modulus and Poisson's ratio we obtained for the graphene with the modified Morse potential function are 0.96 TPa and 0.27, respectively. For all the simulations shown in this paper, the time step is set to be 0.01 ps, and the simulation time is 10 ps (i.e., 1000 time steps).

3.1. Effect of retained component modes

One of the advantages of the CMS-based multiscale approach is the model order reduction of the system by discarding the high-order vibrational modes in each component. For many practical

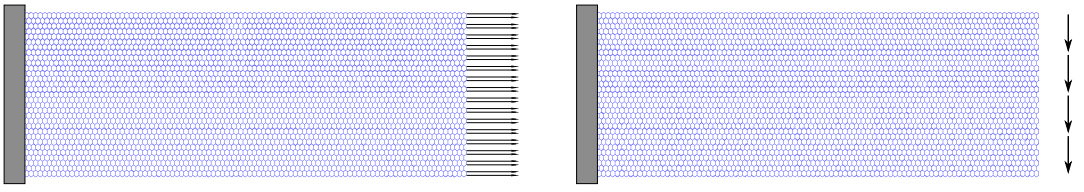

Figure 4. Graphene under external loadings.

DOI: 10.1002/nme

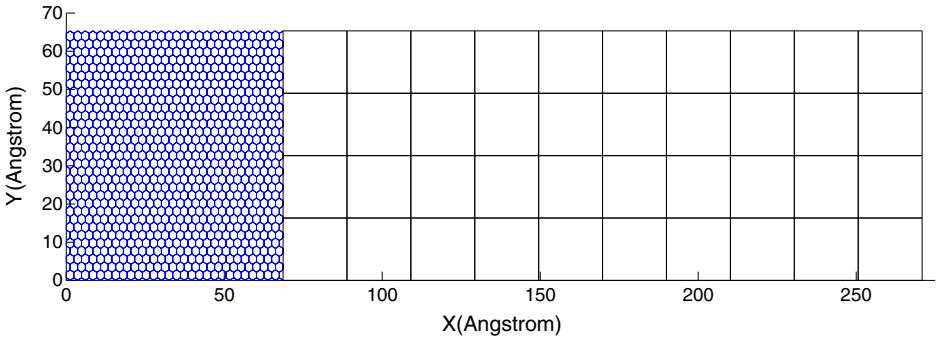

Figure 5. Multiscale model of the perfect graphene.

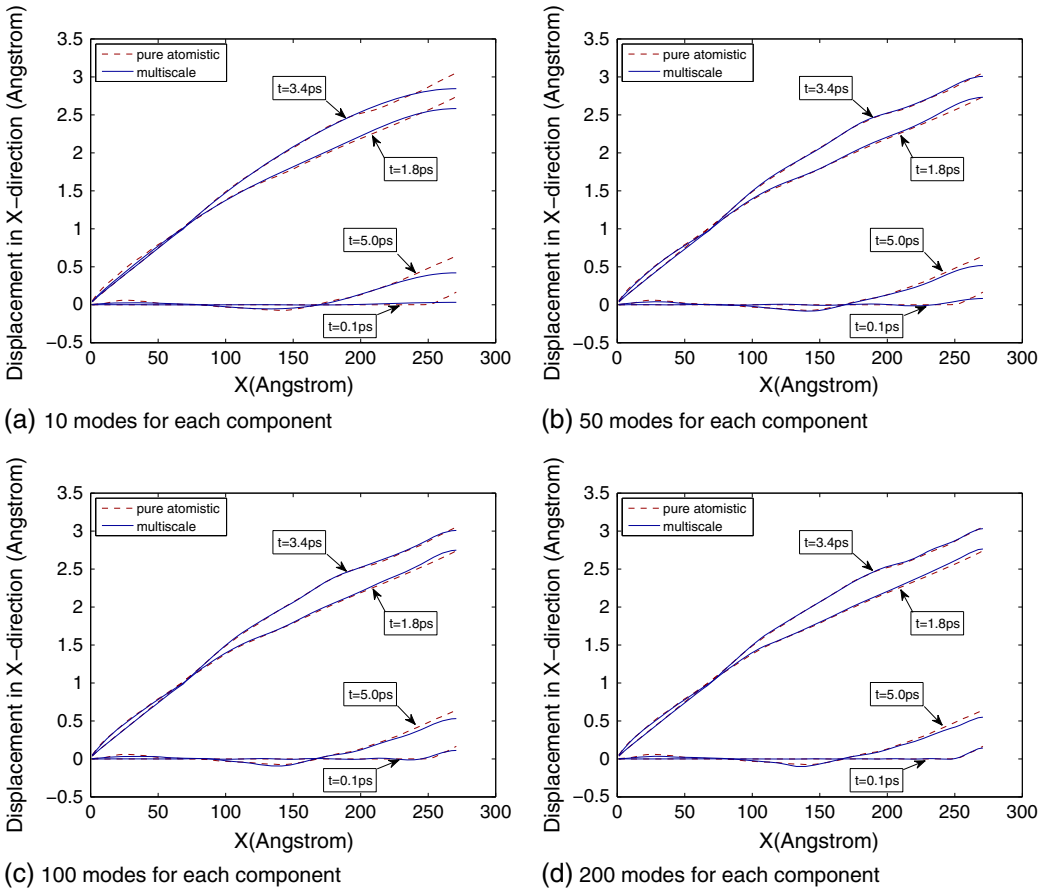

Figure 6. Effect of retained component modes: stretching case. For each component, (a) 10 modes; (b) 50 modes; (c) 100 modes; and (d) 200 modes.

dynamic problems, only the lowest portion of the eigenspectrum needs be retained. In this section, we investigate the effect of number of retained modes on the accuracy of the results.

For both loading cases, we take the atomistic region and the continuum region each as a single component as shown in Figure 5. For both components, we vary the number of modes retained to form the interior modal matrix given in Equation (22). Dynamic results are obtained and compared in Figures 6 and 7 for the stretching and bending cases, respectively. Figure 6 shows the x-displacement profile of the top edge of the graphene ($y = 6.533$ nm) due to the stretching force at different time steps using 10, 50, 100, and 200 retained interior modes. Figure 7 shows, in the

DOI: 10.1002/nme

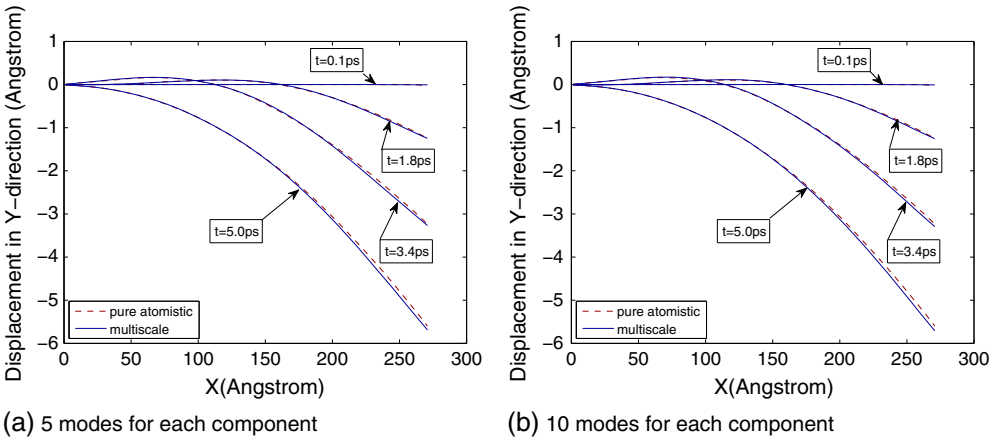

Figure 7. Effect of retained component modes: bending case.

bending case, the y-displacement profile of the top edge at different time steps when 5 and 10 interior modes are retained. In the figures, the solid lines are the results obtained from the CMS multiscale approach, and the dashed lines are the results from pure lattice dynamics simulations. The results show that, for the stretching case, the multiscale results are reasonably accurate when more than 100 modes are retained in both components. Relatively large error is observed for 10 and 50 retained component modes. However, for the bending case, the multiscale results have already converged very well with only 5 retained component modes. The reason for this is that the bending deformation of the structure is dominated by the first few vibrational modes of the graphene, whereas in the stretching case, the elastic wave propagation in the longitudinal direction is participated by more high frequency modes. Thus, more high frequency component modes are needed in the stretching case.

Several advantages of the CMS-based multiscale approach can be observed in the aforementioned results. First, the model order reduction advantage of the multiscale approach is significant. The system DOFs are largely reduced in three ways: (1) a large region of lattice is modeled using continuum elements eliminating a large portion of the atomistic DOFs; (2) a large portion of the high frequency component modes is discarded at the component level (see Equation (22)) because of their negligible contribution to the deformation of the structure; and (3) the DOFs of the system are further reduced at the system level through the mode superposition method as shown in Equation (38). Although feature (1) is the common feature of most multiscale methods, the other two model order reduction features are unique in the CMS-based multiscale approach. Note that, even though 100 modes need to be retained for the atomistic and continuum parts in the stretching case, it is still a very small portion in the eigenspectrum and can be computed efficiently by using smaller components as will be discussed in Section 3.2. Combining the three model order reduction features, the final system, Equation (38), only contains a small set of DOFs. The time integration cost of Equation (38) is negligible compared with that of Equation (5). The advantage becomes more significant when the structure is large, and a large number of time steps are required in the dynamic analysis. The second major advantage of the CMS-based multiscale approach is that the well-known wave reflection problem [17] at the atom–continuum interfaces is inherently eliminated. In the current approach, the global modes synthesized from the atomistic and continuum components are continuous and smooth across the atom–continuum interfaces. The mechanical energy is transmitted across the atom–continuum interfaces through these global modes. The CMS process automatically ensures the compatibility of the elastic waves in the atomistic and continuum components. This point has been confirmed by the multiscale simulation results.

3.2. Effect of component size

The solution of the generalized eigenvalue problem, Equation (21), is the time-consuming part in the CMS. When the DOFs in a component increase, the computational cost of solving Equation (21)

DOI: 10.1002/nme

increases quickly. For this reason, the computational domain is typically decomposed into a set of small components as shown in Figure 2. However, when the components are too small, the overhead of extra matrix operations required by CMS becomes significant. In addition, increasing the number of components leads to an increase of the attachment DOFs in the assembled global system, which will increase the computational cost at the system level. Therefore, in general, there exists an optimal size of the components for the overall efficiency of the calculation. In a previous work, where we extended the CMS approach to calculate the phonon density of states of nanocomposite structures, we found that the optimal size of the components is about 300–400 atoms [39]. In this section, we study the effect of component size on the accuracy of the results.

The graphene model shown in Figure 5 is again used in this section. In Section 3.1, a single component is employed for each of the atomistic and continuum regions. Here, we consider two additional decompositions: a 2×2 and a 5×4 component decomposition for each of the atomistic and continuum regions. The dynamic results of the top edge with stretching and bending deformation for the three component decompositions are shown in Figures 8 and 9. The figures show that the three decomposition schemes give similar results for both loading cases. In addition, we observed that, for the stretching case, to achieve the same accuracy of the 1×1 decomposition with 200 retained component modes, one only needs 50 retained modes per component for the 2×2 decomposition and 10 retained modes per component for the 5×4 decomposition. This result indicates that the total

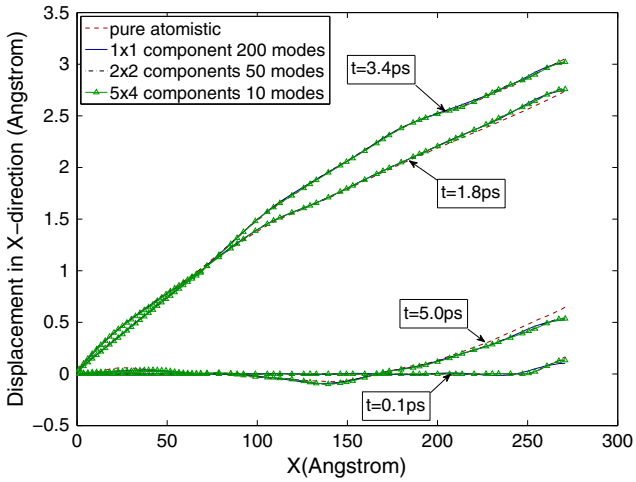

Figure 8. Effect of component size: stretching case.

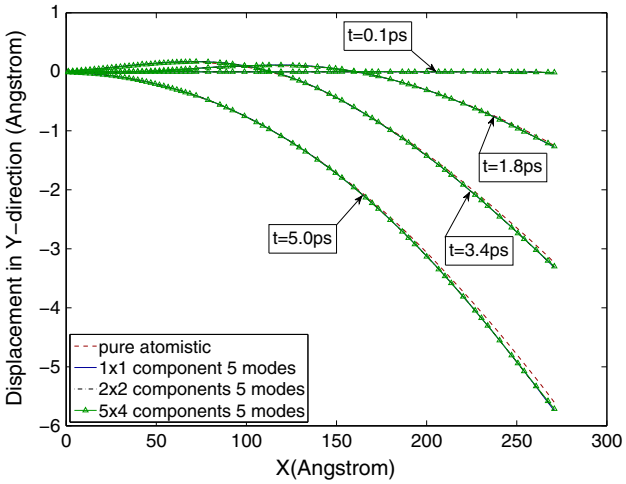

Figure 9. Effect of component size: bending case.

DOI: 10.1002/nme

number of modes required to reach certain accuracy is more or less independent of the component decomposition, that is, the accuracy of the results is insensitive to the component decomposition as long as the total number of modes retained for each region is sufficient. For the bending case, very few component modes are needed to obtain an accurate solution as discussed in Section 3.1. In summary, component size affects the efficiency rather than the accuracy of a CMS multiscale solution.

3.3. Effect of spectral element size

Another modeling parameter in the CMS-based multiscale approach is the spectral element size. By using the master-slave coupling scheme discussed in Section 2, the DOFs of the spectral elements and the atoms at the atom–continuum interfaces need not to be compatible, which allows the use of large elements at the interface. Although this feature provides considerable flexibility in meshing the continuum region, however, it is important to understand the effect of element size on the accuracy of the analysis. In this section, we discretize the continuum part shown in Figure 5 using four different meshes with 2×2, 5×2, 10×4, and 20×8 spectral elements, respectively. Corresponding to the four meshes, the number of atoms on an element edge at the atom–continuum interface is 16, 16, 8, and 4, respectively. The simulation results for the four meshes are shown in Figure 10 (stretching) and Figure 11 (bending). The figures show that the results from the four meshes are

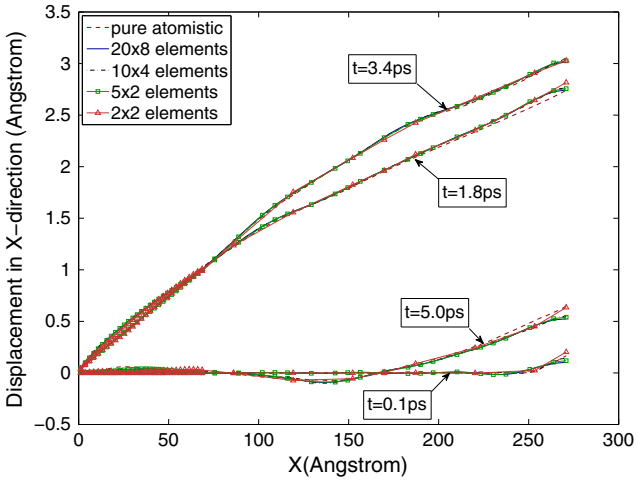

Figure 10. Effect of spectral element size: stretching case.

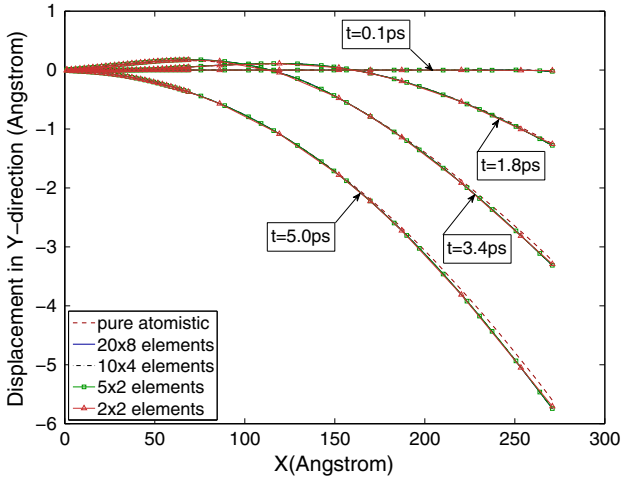

Figure 11. Effect of spectral element size: bending case.

DOI: 10.1002/nme

all very close to the results obtained from the pure atomistic simulations, except that the 2×2 mesh gives a slightly larger error. It is shown that the spectral displacement interpolation in the master-slave coupling at the atom–continuum interface is sufficient. This result also indicates that, in the CMS-based multiscale approach, a spectral element can represent a large number of atoms (each element represents 1350 atoms for the 2×2 mesh in this example). However, it should be pointed out that, as a general principle of numerical analysis, when the displacement variation along the atom–continuum interface is large, smaller elements are necessary to ensure the accuracy.

3.4. Effect of the number of modes in global mode superposition

In Section 2, we propose to employ the mode superposition method at the global level instead of performing direct time integration of Equation (35) to further reduce the computational cost. In the global mode superposition, one also needs to select a set of retained global modes. Here, we investigate the effect of the number of retained global modes. We divide the atomic region and continuum region into 5×4 components each and retain 10 modes for each component, which gives more than 200 modes in each region. Numerical results are obtained for the stretching case by using different number of global modes. Figure 12 shows the top edge displacement in x-direction at four different time steps obtained by using 20, 50, 150, and all of the global modes. It is shown that the mode superposition results with more than 50 modes compare very well with that from the pure atomistic simulation. Even with 20 retained global modes, the error is only slightly larger. Recalling the results shown in Section 3.1, we observe that one needs a lesser number of global modes than the total number of component level normal modes. It is evident that mode superposition can be applied at the global level to further reduce the computational cost. For the bending case, similar comparison is shown in Figure 13, where the y-displacement of the top edge obtained by using the mode superposition method with 5, 10, 20, and all of the global modes is compared with the pure atomistic simulation result. In the bending case, all of the model superposition results are very good, indicating the bending deformation of the graphene only requires a very small set of modes.

3.5. Multiscale dynamic analysis of defective graphene

The goal of the multiscale method is to use atomistic models to describe the regions in a nanostructure where 'nano effects' are significant and use continuum theories to model the regions that are 'bulk-like' so that the 'nano effects' can be captured and the 'bulk-like' regions can be modeled efficiently. In this section, we demonstrate the effectiveness of the CMS-based multiscale approach to achieve this goal through dynamic analysis of a defective graphene. The model of the defective graphene sheet is shown in Figure 14. The defective graphene has the same length

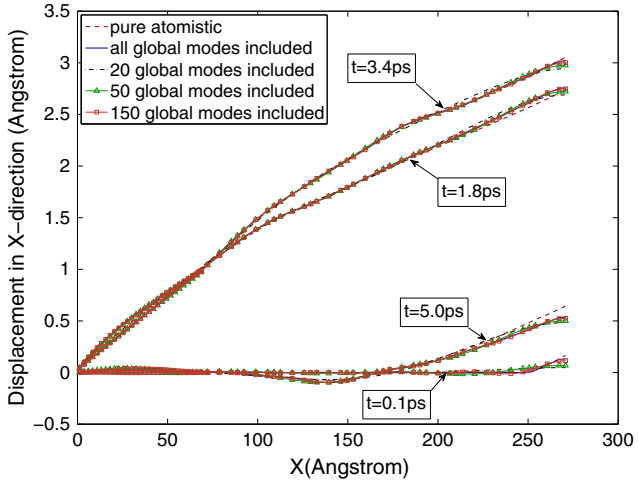

Figure 12. Effect of the number of global modes: stretching case.

DOI: 10.1002/nme

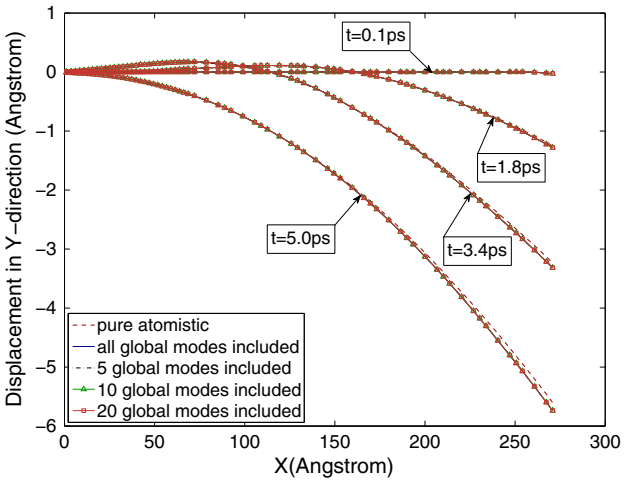

Figure 13. Effect of the number of global modes: bending case.

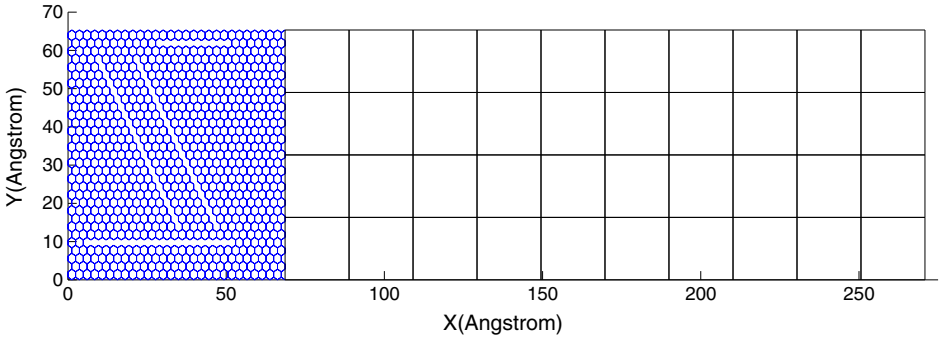

Figure 14. Multiscale model of the defective graphene.

and width and is subjected to the same boundary condition and external loadings as the graphene structures shown in Figure 4. The difference is the four defects in the left part of the graphene where we model as the atomistic region. The right part of the graphene is a perfect lattice where we model using 10×4 spectral elements. We compute the dynamic response of the graphene using two different component decomposition schemes: 1×1 component with 200 retained modes for each region and 2×2 components for each region with 50 retained modes for each component. To evaluate the accuracy of the multiscale simulation results, for each loading case, we also perform an all-atom lattice dynamic simulation for the defective graphene by direct integration of Equation (5).

The results are shown in the Figures 15–18. Figure 15 shows the x-displacement time history of the top right corner node (or atom) of the graphene under the stretch loading. Figure 16 shows the x-displacement of the top edge at four different time steps $t = 0.1$, 1.8, 3.4, and 5 ps. For comparison, the all-atom lattice dynamic results for the perfect graphene structure are also plotted in the figures. The results show that, first, the dynamic behavior of the perfect and defective graphene structures is quite different. The defects in the graphene lead to a significantly larger peak displacement of the structure. In addition, the defects produce a deformation phase change and small oscillations in the overall dynamic response. Therefore, the effect of the defects is significant. Second, comparing the results obtained from the multiscale and pure atomistic simulations for the defective graphene, it is clear that the multiscale simulation results match well with the pure atomistic simulation result. That is, the CMS-based multiscale approach can effectively capture the 'nano effects' in the entire dynamic analysis. For the bending case, the y-directional displacement time history of the top right corner node/atom is shown in Figure 17, and Figure 18 shows the y-displacement of the top edge at

DOI: 10.1002/nme

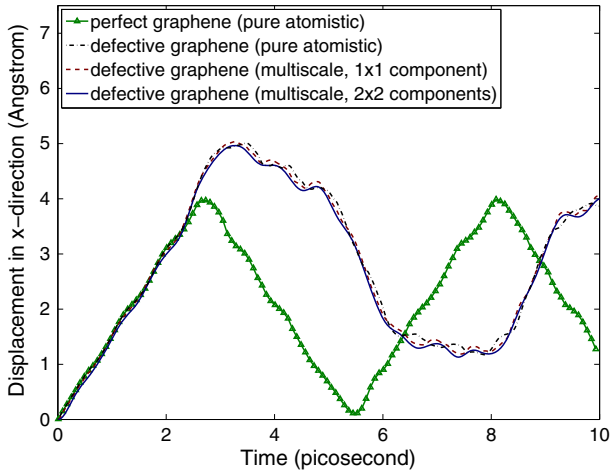

Figure 15. Time history of the top right corner: stretching of the defective graphene.

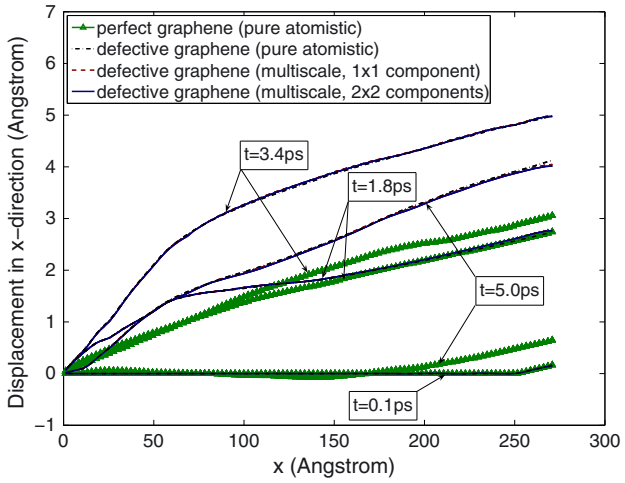

Figure 16. Top edge x-displacement: stretching of the defective graphene.

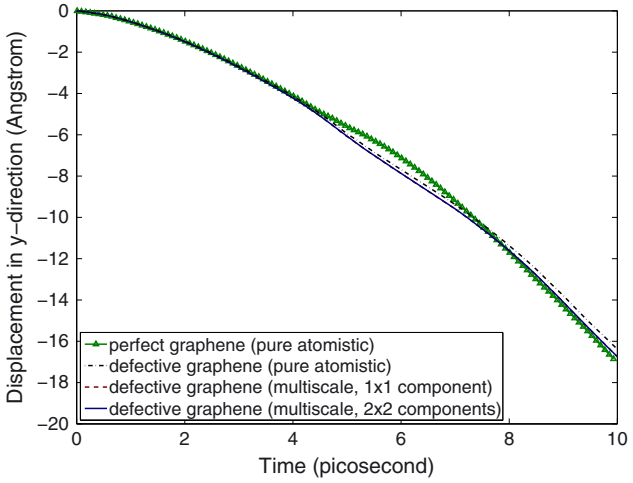

Figure 17. Time history of the top right corner: bending of the defective graphene.

DOI: 10.1002/nme

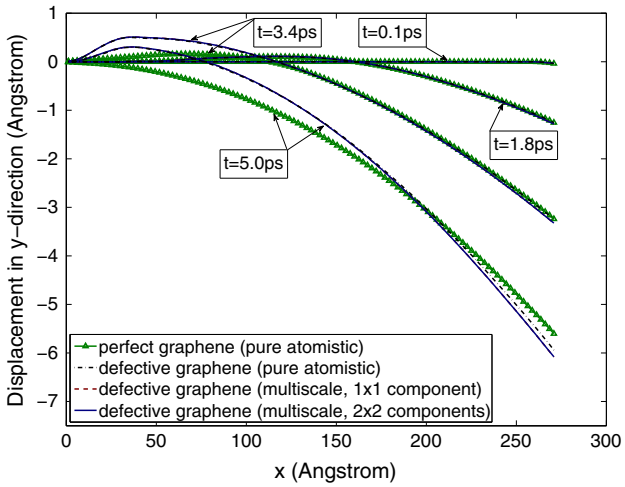

Figure 18. Top edge y-displacement: bending of the defective graphene.

four different time steps. Once again, the effect of defects is considerable, although not as significant as that in the stretching case. The effect is very well captured by the CMS-based multiscale approach under both component decomposition schemes.

4. CONCLUSION

A multiscale CMS modeling and simulation technique combining harmonic lattice dynamics and linear elastodynamics theories is developed and tested. Good agreements between results obtained from the multiscale approach and the full lattice dynamic simulations are observed in numerical examples. The multiscale approach is found to be effective in capturing the 'nano effects' in the dynamic response of nanostructures. Through the mode synthesis procedure in the multiscale approach, the unimportant high-frequency waves are 'filtered out' instead of being reflected back. There is no artificial wave reflection at the atom–continuum interfaces. In addition, the combined global system has the same time scale in the continuum and atomistic regions. Relatively large time steps can be used in the dynamic analysis. Numerical results indicate that the multiscale approach has significant condensation and scaling advantages, and it is well suited for modeling and simulation of large and complex systems. The method allows the individual substructures to each be independently modeled, arbitrarily combined, and combined system response rapidly calculated to determine the global mechanical behavior.

ACKNOWLEDGEMENTS

We gratefully acknowledge the support by the National Science Foundation under grants CMMI-0800474 and CBET-0955096.

REFERENCES

1. Kohlhoff S, Gumbsch P, Fischmeeister H. Crack propagation in b.c.c crystals studied with a combined finite element and atomistic model. *Philosophical Magazine A* 1991; **64**(4):851–878.
2. Broughton JQ, Abraham FF, Bernstein N, Kaxiras E. Concurrent coupling of length scales: Methodology and application. *Physical Review B* 1999; **60**:2391–2403.
3. Atkas O, Aluru NR. A combined continuum/dsmc technique for multiscale analysis of microfluidic filters. *Journal of Computational Physics* 2002; **178**(2):342–372.
4. Deymier PA, Vasseur JO. Concurrent multiscale model of an atomic crystal coupled with elastic continua. *Physical Review B* 2002; **66**(2):134106.
5. Wagner GJ, Liu WK. Coupling of atomistic and continuum simulations using a bridging scale decomposition. *Journal of Computational Physics* 2003; **190**:249–274.

DOI: 10.1002/nme

6. Xiao SP, Belytschko T. A bridging domain method for coupling continua with molecular dynamics. *Computer Methods in Applied Mechanics and Engineering* 2004; **193**:1645–1669.
7. Fish J, Chen W. Discrete-to-continuum bridging based on multigrid principles. *Computer Methods in Applied Mechanics and Engineering* 2004; **193**:1693–1711.
8. Waisman H, Fish J. A space-time multilevel method for molecular dynamics simulations. *Computer Methods in Applied Mechanics and Engineering* 2006; **195**:6542–6559.
9. Tadmor E, Phillips R, Ortiz M. Mixed atomistic and continuum models of deformation in solids. *Langmuir* 1996a; **12**:4529–4534.
10. Tadmor E, Ortiz M, Phillips R. Quasicontinuum analysis of defects in solids. *Philosophical Magazine A* 1996b; **73**(6):4529–4534.
11. Jiang H, Huang Y, Hwang KC. A finite-temperature continuum theory based on interatomic potentials. *Journal of Engineering Materials and Technology* 2005; **127**:408–416.
12. Tang Z, Zhao H, Li G, Aluru NR. Finite-temperature quasicontinuum method for multiscale analysis of silicon nanostructures. *Physical Review B* 2006; **74**(6):064110.
13. Liu B, Huang Y, Jiang H, Qu S, Hwang KC. The atomic-scale finite element method. *Computer Methods in Applied Mechanics and Engineering* 2004; **193**:1849–1864.
14. Fish J, Chen W. Heterogeneous multiscale method: A general methodology for multiscale modeling. *Physical Review B* 2003; **67**:092101.
15. Rudd RE, Broughton JQ. Coarse-grained molecular dynamics and the atomic limit of finite elements. *Physical Review B* 1998; **58**(10):R5893–R5896.
16. Rudd RE, Broughton JQ. Coarse-grained molecular dynamics: Nonlinear finite elements and finite temperature. *Physical Review B* 2005; **72**(14):144104.
17. Liu WK, Karpov E, Zhang S, Park H. An introduction to computational nanomechanics and materials. *Computer Methods in Applied Mechanics and Engineering* 2004; **193**:1529–1578.
18. Fish J. Bridging the scales in nano engineering and science. *Journal of Nanoparticle Research* 2006; **8**:577–594.
19. Wernik JM, Meguid SA. Coupling atomistics and continuum in solids: status, prospects, and challenges. *International Journal of Mechanics and Materials in Design* 2009; **5**(1):79–110.
20. Liu WK, Qian D, Gonella S, Li S, Chen W, Chirputkar S. Multiscale methods for mechanical science of complex materials: Bridging from quantum to stochastic multiresolution continuum. *International Journal of Numerical Methods in Engineering* 2010; **83**:1039–1080.
21. Kudin K, Scuseria G, Yakobson B. C2F, BN, and C nanoshell elasticity from ab initio computations. *Physical Review B* 2001; **64**(23):235406.
22. Nayfeh AH, Mook DT. *Nonlinear Oscillations*. John Wiley and Sons: New York, 1979.
23. Iwatsubo T, Shimbo K, Kawamura Sh. Nonlinear vibration analysis of a rotor system using component mode synthesis method. *Archive of Applied Mechanics* 2003; **72**:843–855.
24. Maradudin AA, Montroll EW, Weiss GH, Ipatova IP. *Theory of Lattice Dynamics in the Harmonic Approximation, in Solid State Physics, Suppl. 3*. Academic Press: New York, 1971; 244–256.
25. Girifalco LA, Lad RA. Energy of cohesion, compressibility, and the potential-energy functions of the graphite system. *Journal of Chemical Physics* 1956; **25**:693.
26. Morse PM. Diatomic molecules according to the wave mechanics. ii. vibrational levels. *Physical Review* 1929; **34**:57–64.
27. Tersoff J. Empirical interatomic potential for carbon, with applications to amorphous carbon. *Physical Review Letter* 1988; **61**:2879–2882.
28. Brenner DW. Empirical potential for hydrocarbons for use in simulating the chemical vapor deposition of diamond films. *Physical Review B* 1990; **42**:9458–9471.
29. Stillinger FH, Weber TA. Computer simulation of local order in condensed phases of silicon. *Physical Review B* 1985; **31**:5262–5271.
30. Belytschko T, Xiao SP, Schatz GC, Ruoff RS. Atomistic simulations of nanotube fracture. *Physical Review B* 2002; **65**(23):235430.
31. Mathew N, Picu RC, Bloomfield M. Concurrent coupling of atomistic and continuum models at finite temperature. *Computer Methods in Applied Mechanics and Engineering* 2011; **200**(5-8):765–773.
32. Tuckerman ME. *Statistical Mechanics: Theory and Molecular Simulation*. Oxford University Press: New York, 2010.
33. Patera AT. A spectral element method for fluid dynamics: Laminar flow in a channel expansion. *Journal of Computational Physics* 1984; **54**:468–488.
34. Karniadakis GE, Sherwin SJ. *Spectral/hp Element Methods for CFD*. Oxford University Press: New York, 1999.
35. Canuto C, Hussaini MY, Quarterino A, Zang TA. *Spectral Methods: Fundamentals in Single Domains*. Springer: New York, 2006.
36. Gottlieb D, Orszag SA. *Numerical Analysis of Spectral Method: Theory and Applications*. SIAM: Philadelphia, 1977.
37. Hurty WC. Dynamic analysis of structural systems using component modes. *AIAA Journal* 1965; **3**(4):678–685.
38. Craig RR, Kurdila AJ. *Fundamentals of Structural Dynamics*. John Wiley and Sons: New York, 2006.
39. Li G. A multilevel component mode synthesis approach for the calculation of the phonon density of states of nanocomposite structures. *Computational Mechanics* 2008; **42**(4):593–606.
40. Li H, Li G. Component mode synthesis approaches for quantum mechanical electrostatic analysis of nanoscale devices. *Journal of Computational Electronics* 2011; **10**(3):300–313.

DOI: 10.1002/nme

41. Craig RR, Jr, Bampton MCC. Coupling of substructures for dynamic analysis. *AIAA Journal* 1968; **6**(7):1313–1319.
42. Craig RR, Chang CJ. Free-interface methods of substructure coupling for dynamic analysis. *AIAA Journal* 1976; **14**(11):1633–1635.
43. Shyu WH, Gu J, Hulbert GM, Ma ZD. On the use of multiple quasi-static mode compensation sets for component mode synthesis of complex structures. *Finite Element in Analysis and Design* 2000; **35**:119–140.
44. Xu M, Gracie R, Belytschko T. Multiscale modeling with extended bridging domain method. In *In Bridging the Scales in Science and Engineering*, Fish J (ed.). Oxford Press, 2009.
45. Belytschko T, Xiao SP. Coupling methods for continuum model with molecular model. *International Journal for Multiscale Computational Engineering* 2003; **1**:115–126.
46. Sert C, Beskok A. Spectral element formulations on non-conforming grids: A comparative study of pointwise matching and integral projection methods. *Journal of Computational Physics* 2006; **211**(1):300–325.
47. Tsai CT, Szabo BA. A constraint method-a new finite element technique. *NASA Technical Memorandum, NASA, TM X-2893*, 1973, pages 551–568.

DOI: 10.1002/nme